Constraint of the CO2 rise by new atmospheric carbon isotopic measurements during the last deglaciation

Anna Lourantou, Jošt V. Lavrič, Peter Köhler, Jean-Marc Barnola, Didier Paillard, Elisabeth Michel, Dominique Raynaud, Jérôme Chappellaz

HAL Id: insu-00562248
https://insu.hal.science/insu-00562248

Submitted on 5 Mar 2021

Constraint of the CO_2 rise by new atmospheric carbon isotopic measurements during the last deglaciation

Anna Lourantou,[1] Jošt V. Lavrič,[1,2] Peter Köhler,[3] Jean-Marc Barnola,[1,4] Didier Paillard,[2] Elisabeth Michel,[2] Dominique Raynaud,[1] and Jérôme Chappellaz[1]

[1] The causes of the ~80 ppmv increase of atmospheric carbon dioxide (CO_2) during the last glacial-interglacial climatic transition remain debated. We analyzed the parallel evolution of CO_2 and its stable carbon isotopic ratio ($\delta^{13}CO_2$) in the European Project for Ice Coring in Antarctica (EPICA) Dome C ice core to bring additional constraints. Agreeing well but largely improving the Taylor Dome ice core record of lower resolution, our $\delta^{13}CO_2$ record is characterized by a W shape, with two negative $\delta^{13}CO_2$ excursions of 0.5‰ during Heinrich 1 and Younger Dryas events, bracketing a positive $\delta^{13}CO_2$ peak during the Bølling/Allerød warm period. The comparison with marine records and the outputs of two C cycle box models suggest that changes in Southern Ocean ventilation drove most of the CO_2 increase, with additional contributions from marine productivity changes on the initial CO_2 rise and $\delta^{13}CO_2$ decline and from rapid vegetation buildup during the CO_2 plateau of the Bølling/Allerød.

1. Introduction

[2] Atmospheric CO_2 is the most important anthropogenic greenhouse gas and arguably the largest contributor to the current global warming [*Intergovernmental Panel on Climate Change*, 2007]. The monitoring of its stable carbon isotopic ratio ($\delta^{13}CO_2$) evolution is useful for the identification of biogeochemical processes driving the observed variations in CO_2. Former studies [*Friedli et al.*, 1986; *Francey et al.*, 1999] provided decisive evidence for the manmade origin of the CO_2 rise during the last 200 years, based on a ~1.5‰ decline of $\delta^{13}CO_2$ to its modern value of −7.8‰. This decrease is caused by the ^{13}C-depleted signature of the two major anthropogenic CO_2 sources, fossil fuel burning and carbon release from deforestation, having $\delta^{13}CO_2$ values of ~−30‰ and −25‰, respectively.

[3] In contrast, natural changes in CO_2, such as the 80 ppmv rise over Termination I (hereafter TI), i.e., the transition from the Last Glacial Maximum (LGM) ~20 kyr B.P. to the Early Holocene (EH, ~10 kyr B.P.), are still not well understood. Modeling studies attribute it to various oceanic processes, but without consensus on their relative importance [*Broecker and Peng*, 1986; *Watson and Naveira Garabato*, 2006]. Two major mechanisms in the ocean are usually invoked to explain the CO_2 glacial-interglacial (G-IG) changes: (1) a physical one, mainly related to Southern Ocean ventilation changes eventually releasing during Terminations old carbon stored in the deep ocean during the preceding glaciation [*Toggweiler*, 1999] and (2) a biological one, involving the efficiency of nutrient utilization by phytoplankton in the austral ocean, with decreased efficiency (and thus lower CO_2 uptake) when atmospheric dust fertilization gets reduced [*Archer et al.*, 2000; *Sigman and Boyle*, 2000]. For more than 3 decades, scientists tried to disentangle the relative role of these or alternative processes, such as changes in oceanic pH and carbonate compensation [*Archer et al.*, 2000], in the evolution of atmospheric CO_2. Currently, few models can reproduce the observed amplitude in G-IG CO_2 rise; they succeed only if all processes relevant on these timescales are considered [*Köhler et al.*, 2005a; *Brovkin et al.*, 2007].

[4] To validate their hypothesis or to propose alternative ones, more observational constraints are needed. Paleoatmospheric $\delta^{13}CO_2$ makes one of them and is central to our study. So far, a unique record of atmospheric $\delta^{13}CO_2$ through TI (including ~15 measurements) has been obtained from the Taylor Dome (TD) ice core [*Smith et al.*, 1999; SM1999 hereafter], filling the time jigsaw between LGM and EH first produced from the Byrd core [*Leuenberger et al.*, 1992]. Although of coarse resolution, the TD $\delta^{13}CO_2$ record has already been used to evaluate the output of several carbon (C)

[1]Laboratoire de Glaciologie et Géophysique de l'Environnement, Université Joseph Fourier–Grenoble, CNRS, St Martin d'Hères, France.

[2]Laboratoire des Sciences du Climat et de l'Environnement, IPSL, Université Versailles-St Quentin, CNRS, Gif-sur-Yvette, France.

[3]Alfred Wegener Institute for Polar and Marine Research, Bremerhaven, Germany.

[4]Deceased 2009.

cycle models [*Schulz et al.*, 2001; *Brovkin et al.*, 2002; *Köhler et al.*, 2005a; *Obata*, 2007]. For instance [*Obata*, 2007], using a coupled climate-C cycle model, simulates a decrease in net primary productivity and soil respiration during the Younger Dryas, in agreement with a combined increase of atmospheric CO_2 and minimum of $\delta^{13}CO_2$ observed in the TD ice core at that time. [*Brovkin et al.*, 2002] emphasize the role of the G-IG reduced biological pump to explain the simultaneous CO_2 increase and $\delta^{13}CO_2$ decrease suggested by the TD data during the early part of the Termination.

[5] In this study we (1) present a new highly resolved record of CO_2 and $\delta^{13}CO_2$ across TI from the European Project for Ice Coring in Antarctica (EPICA) Dome C (EDC) ice core, (2) compare it to existing ice core data (CO_2 from EDC [*Monnin et al.*, 2001] and $\delta^{13}CO_2$ from TD (SM1999)), (3) propose a qualitative scenario on the causes of the deglacial CO_2 rise, based on a comparison with other proxies, and (4) test this scenario with two C cycle box models [*Köhler et al.*, 2005a; *Paillard et al.*, 1993].

2. Method

[6] A detailed description of the experimental method is provided by *Lourantou* [2009]. In short, 40–50 g of ice are cut in a cold room, removing about 3 mm of the original sample surface in order to avoid artifacts due to gas diffusion at the atmosphere/ice interface [*Bereiter et al.*, 2009]. The sample is then sealed in a stainless steel ball mill, evacuated and crushed to fine powder. The gas liberated from the bubbles is expanded over a −80°C ethanol/liquid nitrogen (LN) water trap onto an evacuated 10 cm^3 sample loop. From there it is flushed by an ultra pure helium stream through a partially heated glass trap where the CO_2 is frozen out at LN temperature (−196°C). The trapped CO_2 is then transferred into another ultra pure helium stream of lower flow rate, to be cryofocused on a small volume uncoated glass capillary tubing at LN temperature. The subsequent warming of the capillary allows the gas transfer with ultra-pure helium into a gas chromatograph to separate the CO_2 from residual impurities (e.g., N_2O having the same mass over charge ratio as CO_2, [*Ferretti et al.*, 2000]), its subsequent passage through an open split system to be finally directed to the isotope ratio mass spectrometer (IRMS, Finnigan MAT 252).

2.1. Signal Determination and Correction

2.1.1. Standard Gases

[7] The CO_2 mixing ratio in the ice samples is deduced from a linear regression between the varying pressure of several external standard gas injections and the corresponding CO_2 peak amplitude measured by the IRMS. The external standard gas has been prepared at CSIRO (Australia) and contains CO_2 = 260.3 ± 0.2 ppmv in dry air, with a $\delta^{13}CO_2$ = −6.40 ± 0.03‰ versus the international standard Vienna Pee-Dee Belemnite, VPDB ($\delta^{13}CO_2$ is reported in standard δ notation as the per mil (‰) difference between the stable carbon isotope composition of the sample and VPDB; $\delta^{13}C$ = $[(^{13}C/^{12}C)_{sample}/(^{13}C/^{12}C)_{VPDB}] - 1$). It is preconcentrated and transferred throughout the system similarly as ice core gas samples. Each sample or external standard introduction in the

IRMS is bracketed with injections of a pure CO_2 standard reference gas (internal standard, ATMO MESSER, $\delta^{13}C$ = −6.5 ± 0.1‰ versus VPDB) through another open split, to calibrate the IRMS and to correct for instrumental drift at the scale of a few minutes. Each spectrogram contains the sample/external standard peak, juxtaposed with peaks eluted from the internal standard gas. The mass over charge (m/z) 44 peak height of the internal standard injected with each gas sample is fitted as closely as possible to the expected CO_2 peak height from the ice core gas sample or CSIRO standard, in order to avoid linearity corrections due to the IRMS response. The amount of the external standard gas processed before each ice core gas sample expansion is also adjusted to the expected gas sample peak height for the same reason.

[8] During the experimental protocol, the CSIRO external standard gas is processed seven times before, during and after the ice core gas sample measurement. The latter is usually processed several times, with three consecutive expansions of the same sample gas stored in the extraction container. Thus each data point corresponds to the average value of three replicate measurements of the same extracted gas. The pooled standard deviation on these replicates is 0.98 ppmv for CO_2 and 0.098‰ for $\delta^{13}CO_2$, while the pooled standard deviation on the routine daily processing of the CSIRO external standard gas is 0.90 ppmv for CO_2 and 0.15‰ for $\delta^{13}CO_2$. The last number does not directly translate to ice core measurements, as it integrates the large daily range of standard gas amount processed through the system and thus the nonlinearity of the IRMS response, whereas each ice core gas sample is measured for $^{13}CO_2$ against a single standard gas peak having a comparable CO_2 amplitude.

[9] On a daily basis, a correction is applied on the carbon isotopic ratios obtained on ice samples, based on the deviation observed between the external air standard measurements and the attributed CSIRO value. The correction relies on the seven external air standard injections processed before the ice sample, in between the three expansions of the ice sample, and after the ice sample. On average, a systematic deviation of −0.30‰ from the attributed CSIRO value was observed over the whole EDC measurement period, without any systematic trend from day to day [*Lourantou*, 2009].

2.1.2. Blank Tests

[10] Three different "blank tests" were conducted throughout the sampling period, with the following differences compared with the procedure described above:

[11] 1. No gas introduced in the sample loop. Results show a very low blank (residual traces of CO_2 in the transfer lines and carrier gas): we obtain on average (n = 35) a CO_2 amplitude equivalent to 0.33–1.7% of the external standard gas peak heights.

[12] 2. A known quantity of external standard gas is introduced in an empty ice mill and then processed to evaluate possible fractionations when expanding a known gas from the cold mill to the sample loop.

[13] 3. A known quantity of external standard gas is introduced in the ice mill together with artificial bubble-free ice and then processed after crushing, to reproduce conditions similar to those of a real ice core sample.

Table 1. Blank Test Results of the Experimental Setup on Standard Gas With Their 1σ Standard Deviation and the Number of Tests

Test	CO_2 (ppmv)	$\delta^{13}CO_2$ (‰)	Test Number (n)
II	261.1 ± 1.2	-6.4 ± 0.1	5
III	261.4 ± 1.8	-6.7 ± 0.1	14

[14] Results of the last two blank tests are shown in Table 1. CO_2 results of the two blank tests are identical to the external standard gas value within the analytical uncertainty (Table 1). The same applies for $\delta^{13}CO_2$ in test (II). On the other hand, test (III) with bubble-free ice give an average $\delta^{13}CO_2$ depleted by ~0.3‰ compared to the CSIRO value. This may arise from a small fractionation taking place when a gas sample including a small amount of water vapor (vapor pressure at $-60°C$, i.e., the temperature in the container) is transferred into the vacuum line. We decided not to apply such correction to our measurements, due to insufficient statistics. The absolute values presented here should thus be considered with caution, until we obtain good statistics on applying our system for instance on numerous samples of preindustrial and industrial ice. The $\delta^{13}CO_2$ signal for the past 1000 years is well established [*Francey et al.*, 1999]; numerical deviations obtained with our system would confirm or infirm the need for such blank correction. If any, such small possible bias does not affect the relative $\delta^{13}CO_2$ changes observed throughout Termination I. Our results can thus safely be compared one to the other and discussed within the experimental uncertainty range, being on average of 0.1‰.

2.2. Corrections Due to Diffusion Processes in the Firn Column

[15] Gas molecules in interstitial firn air mostly fractionate by molecular diffusion, in addition to gravitational settling. The latter provokes a preferential accumulation of heavier molecules (for the case of gases) or isotopologues (for the case of isotopes) at the bottom of the firn column compared with the atmosphere [*Craig et al.*, 1988; *Schwander et al.*, 1993]. The fractionation is proportional to the mass difference between the involved gases; the one between $^{13}CO_2$ and $^{12}CO_2$, is identical to ^{15}N versus ^{14}N of N_2. Therefore we use $\delta^{15}N$ of N_2 data from the EDC core, or modeled $\delta^{15}N$ of N_2 from an empirical relationship with δD in the ice (both provided by *Dreyfus et al.* [2010]) to correct $\delta^{13}CO_2$ for gravitational fractionation. The CO_2 mixing ratio was also corrected for gravitational fractionation, following [*Etheridge et al.*, 1996].

[16] Using measured or modeled $\delta^{15}N$ of N_2 changes the correction by a maximum of 0.03–0.04‰. We finally used the modeled $\delta^{15}N$ of N_2, due to the limited depth coverage of the measured $\delta^{15}N$ of N_2 data. For CO_2, the gravitational correction varies from -1.16 to -2.20 ppmv, while for $\delta^{13}CO_2$, it amounts between -0.41‰ (glacial ice) and -0.55‰ (Holocene ice). Note that such correction was not applied to the previous EDC CO_2 record [*Monnin et al.*, 2001].

[17] The difference of diffusion coefficient in air between $^{12}CO_2$ and $^{13}CO_2$ generates changes in the $\delta^{13}CO_2$ signal in firn air and trapped bubbles due to molecular diffusion, whenever CO_2 varies in the atmosphere, even when atmospheric $\delta^{13}CO_2$ remains unchanged. The magnitude of this effect can be calculated with firn air diffusion models [*Trudinger et al.*, 1997]. Under present-day conditions when CO_2 increases by about 2 ppmv/yr, the diffusion correction on firn air and trapped bubbles composition amounts to about 0.10‰ on a 70 m thick firn column [*Trudinger et al.*, 1997]. Since the correction is at first order proportional to the CO_2 rate of change, and as the largest observed CO_2 rate of change during TI is about 20 times smaller than the present-day increasing rate [*Joos and Spahni*, 2008], the molecular diffusion correction would amount to less than 0.01‰ on the EDC $\delta^{13}CO_2$ profile, and is thus neglected here.

[18] A final possible correction on gas mixture measured in air bubbles is related to thermal fractionation [*Severinghaus et al.*, 2001; *Grachev and Severinghaus*, 2003]. As surface temperature changes at EDC were too slow to generate large thermal gradients and gas fractionation, and as no thermal anomaly was detected in the measured $\delta^{15}N$ of N_2 at EDC, no thermal correction was applied to the measured $\delta^{13}CO_2$.

2.3. Reliability of the Record

[19] Greenland ice has been found to include in situ produced CO_2, involving either carbonate/acid reaction or oxidation of organic compounds [*Anklin et al.*, 1995; *Tschumi and Stauffer*, 2000; *Ahn et al.*, 2004]. No such artifact has been observed so far in Antarctic ice, probably due to the much lower impurity content compared with Greenland ice.

[20] All samples measured here originate from the EDC ice core drilled at Concordia Station in Antarctica (75°06′S, 123°21′E; 3233m. above sea level) during the field season 1997–98. Experimental or chemical artifacts affecting CO_2 and/or $\delta^{13}CO_2$ can be detected when the scatter of duplicates exceeds 3σ of the external precision of the analytical technique. None of the investigated depth levels show such anomaly, thus indicating that the signal can be interpreted within the experimental uncertainty limits. On the other hand, one of the bag sections (dated at 12.6 kyr B.P. in the EDC3_gas_a scale [*Loulergue et al.*, 2007]; for comparison, see next section) provided reproducible mixing and isotopic ratios on duplicate measurements, but its average $\delta^{13}CO_2$ differed from neighboring bags (including trapped gas younger or older by less than 100 years) by more than 0.2‰. We hypothesize that the corresponding core section has been affected by anomalous storage and local transportation conditions (exposure to warm temperatures), leading to a suspicious result. We thus discard it for the interpretation that follows.

2.4. Age Scale

[21] All EDC records are officially dated on the EDC3-beta6 [*Parrenin et al.*, 2007] and EDC3_gas_a [*Loulergue et al.*, 2007] age scales for ice and gas data, respectively. However, in order to compare our EDC data with data from other cores (of marine or polar origin) and with

Table 2a. Tie Points Between the EDC3_gas_a and GICC05 Timescales[a]

EDC3_gas_a Age[b] (Years B.P.)	GICC05 Gas Age[c] (Years B.P.)	CH$_4$ Value (ppbv)	Event Description
7,890	8,240	590	CH$_4$ minimum during Holocene
11,330	11,680	560	CH$_4$ midrise/ending of YD
11,920	12,330	460	CH$_4$ YD minimum
12,340	12,790	540	CH$_4$ mid decrease/ending of B/A
13,070	13,600	670	B/A CH$_4$ peak
14,010	14,640	570	CH$_4$ midrise/toward B/A
15,870	16,200	470	CH$_4$ peak
17,790	17,800	370	CH$_4$ drop
19,690	19,670	350	CH$_4$ drop
21,220	21,100	350	CH$_4$ drop during LGM

[a]Using the ANALYSERIES Software [*Paillard et al.*, 1996].
[b]*Loulergue et al.* [2007].
[c]*EPICA Community Members et al.* [2006], *Andersen et al.* [2007], and *North Greenland Ice Core Project Members* [2004].

model simulations constrained by other data sets, we synchronized both EDC and TD, using CH$_4$ as a time marker, to the newest Greenland chronology GICC05 [*Rasmussen et al.*, 2006], using the Analyseries software [*Paillard et al.*, 1996]. The tie points for each core are presented in Tables 2a and 2b. The synchronized TD chronology is less constrained than the EDC one, due to the poorer time resolution of the TD CH$_4$ record [*Köhler et al.*, 2005a]. The EDC ice chronology (e.g., δD in Figure 1a) is obtained by combining the CH$_4$ gas age fit on the GICC05 timescale and the Δage calculated with the EDC3beta6 chronology.

3. Results

[22] Sixty three samples were measured from 50 different depth intervals (345 to 580 m of depth), covering the time period from 9 to 22 kyr B.P. This provides a mean time resolution of 220 years through the transition, whereas the previous published TD record offered a mean time resolution of only ~1000 years. Duplicate analyses of thirteen samples cut on the same ice bags yielded a reproducibility (1σ) of 0.99 ppmv and 0.1‰, respectively. The good correspondence between the reproducibility of CSIRO external standard measurements and of duplicate measurements of neighboring ice samples gives confidence in our main ice core signal structure. Measurements were performed exclusively on clathrate-free ice samples, at depths shallower than 600 m.

3.1. Comparison With Previous Data Sets

[23] The new CO$_2$ and $\delta^{13}CO_2$ data sets are plotted together with previously published data (CO$_2$, δD and CH$_4$) from EDC [*Monnin et al.*, 2001; *Jouzel et al.*, 2007; *Loulergue et al.*, 2008] and TD [SM1999; *Brook et al.*, 2000], as well as the $\delta^{18}O$ data from North Greenland Ice Core Project (NGRIP) core [*North Greenland Ice Core Project Members*, 2004] in Figure 1. The agreement between the detailed trends of both CO$_2$ records from the same EDC core [*Monnin et al.*, 2001] is remarkable (R^2 = 0.996; see Figure 1d). Minor differences in the absolute values result from the use of different CO$_2$ international

scales (SIO for the data of [*Monnin et al.*, 2001], and CSIRO in this study) and from the gravitational correction only applied to our data set. The high temporal resolution allows the division of TI into four subperiods (SP-I to SP-IV) as initiated by [*Monnin et al.*, 2001], characterized by different rates of CO$_2$ change. With 40 measurements throughout TI, the data resolution is improved by more than a factor of two compared with SM1999 (Figures 1d and 1e). Overall, the EDC and TD $\delta^{13}CO_2$ show similar mean values and trends in the course of TI, with 75% of the TD data falling within the 1σ EDC uncertainty (taking into account dating errors in the comparison). On the other hand, the TD CO$_2$ data are more scattered than the EDC ones.

[24] Both EDC and TD $\delta^{13}CO_2$ records reveal a W shape through TI, much more obvious in this new EDC record, with maximum amplitude of contiguous change of ~0.5‰, and a full $\delta^{13}CO_2$ range of 0.7‰. The better time resolution of the EDC profile reveals a more structured signal than the TD one within the ~0.1‰ experimental uncertainty, depicting notably faster transitions. This permits for the first time a detailed comparison of the isotopic signal with the changes in the CO$_2$ slope, within an uncertainty range comparable to the TD data set (given as $\pm$ 0.085‰ by SM1999). The latter value is probably a low estimate, as the atmospheric N$_2$O trend, needed to apply a correction on the TD $\delta^{13}CO_2$ measurements, was considered linear through the deglaciation, whereas the real N$_2$O signal reconstructed since shows a much different structure [*Flückiger et al.*, 1999]. We remind that in our case no such N$_2$O correction is needed (for comparison, see section 2).

3.2. CO$_2$ and $\delta^{13}CO_2$ Trends Throughout TI

[25] Figures 1d and 1e reveal a much different behavior between CO$_2$ and $\delta^{13}CO_2$: while CO$_2$ mostly shows linear trends within each subperiod (SP), $\delta^{13}CO_2$ exposes a more dynamic pattern during the SPs II to IV, with spikes and troughs superimposed on relatively stable boundary values.

[26] LGM $\delta^{13}CO_2$ also shows a large variability whereas CO$_2$ bears little changes, a feature already observed with similar amplitude in previous data sets [*Leuenberger et al.*, 1992; SM1999]. Part of the LGM $\delta^{13}CO_2$ variability parallels very small fluctuations in the CO$_2$ rate of change observed in the [*Monnin et al.*, 2001] data set. Between

Table 2b. Tie Points Between TD and GICC05 Age Scales[a]

TD Gas Age (Years B.P.)	GICC05 Gas Age (Years B.P.)	CH$_4$ Value (ppbv)	Event Description
8,300	8,290	570	CH$_4$ minimum during Holocene
11,690	11,660	660	CH$_4$ peak after YD
11,890	11,860	430	CH$_4$ YD minimum
12,910	12,830	600	CH$_4$ mid decrease/ending of B/A
13,570	13,430	670	B/A CH$_4$ peak
14,880	14,790	510	Just before the B/A CH$_4$ rise
16,770	16,200	500	CH$_4$ peak before B/A
26,470	22,810	420	CH$_4$ peak during LGM

[a]Using the same software of *Paillard et al.* [1996]. The TD core was initially plotted versus GISP2 age scale [*Brook et al.*, 2000]. GISP2 is almost synchronous to GICC05; still, for the LGM time period, GISP2 had to be rescaled.
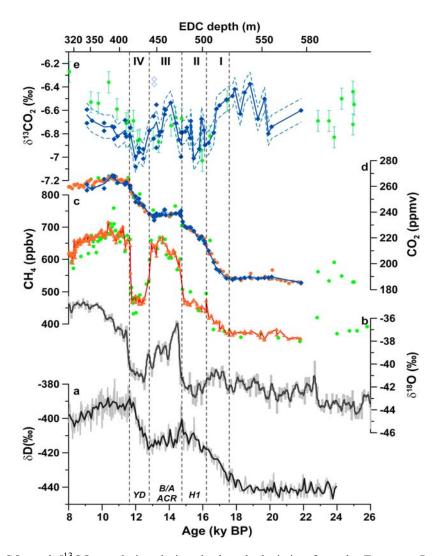
Figure 1. CO_2 and $\delta^{13}CO_2$ evolution during the last deglaciation from the European Project for Ice Coring in Antarctica (EPICA) Dome C (EDC) ice core, superimposed with other ice core data: (a) δD of ice in EDC (gray line [*Jouzel et al.*, 2007]), averaged over 500 years (black line [*EPICA Community Members et al.*, 2006]); (b) $\delta^{18}O$ of North Greenland Ice Core Project (NGRIP) ice [*North Greenland Ice Core Project Members*, 2004], with a running average over 500 years (dark gray line); (c) atmospheric CH_4 mixing ratio (red line and triangles, EDC [*Loulergue et al.*, 2008]; green dots, TD [*Brook et al.*, 2000]); (d) atmospheric CO_2 mixing ratio (red line and dots, EDC [*Monnin et al.*, 2001]; blue line and diamonds, this study; green dots, TD [*Smith et al.*, 1999]); and (e) $\delta^{13}CO_2$ data (blue line and diamonds, this study; green dots, TD [*Smith et al.*, 1999]). When duplicate measurements were performed, the line runs through the mean. The dotted blue lines in Figure 1e correspond to the 1σ (0.1 ‰ average) uncertainty envelope. The two blue open diamonds indicate a suspicious result that we discarded in the discussion. All gas records are plotted versus the Greenland GICC05 age scale. The upper x axis represents the EDC depth for the gas records, and δD is plotted on a chronology combining the CH_4 fit to GICC05 and the EDC3 Δage [*EPICA Community Members et al.*, 2006]. The vertical dotted lines correspond to boundaries between different CO_2 rates of change during the deglaciation, as defined by *Monnin et al.* [2001], adapted to the new age scale. The time periods in between are noted SP-I to SP-IV. YD, Younger Dryas; B/A, Bølling/Allerød; ACR, Antarctica Cold Reversal; H1, Heinrich 1.

22 and 17.6 kyr B.P., we obtain an average of 188 ± 1 ppmv for CO_2 and $-6.6 \pm 0.1‰$ for $\delta^{13}CO_2$ (n = 10).

[27] The evolution of both CO_2 and $\delta^{13}CO_2$, with respect to Northern and Southern Hemisphere (hereafter NH and SH, respectively) climatic events, can be summarized as follows:

[28] 1. Subsequent to the late LGM (22−17.6 kyr B.P.), the early part of TI (SP-I, from 17.6 to 16.2 kyr B.P.) is associated with a 25 ppmv rise of CO_2 and a 0.3‰ fall of $\delta^{13}CO_2$.

[29] 2. SP-II (16.2 to 14.7 kyr B.P.), during which the Heinrich 1 (H1) event ends in the NH (as deduced from ice-rafted debris in the North Atlantic [*Hemming*, 2004] and also seen in NGRIP temperature data in Figure 1b), reveals a two-step CO_2 rise; the first occurs until 15 kyr B.P. with a progressive 14 ppmv increase and the second with a 12 ppmv rise within only 300 years. Meanwhile, $\delta^{13}CO_2$ experiences an oscillation of ~0.2‰ amplitude and reaches a minimum of $-7.0 \pm 0.1‰$ at about 15.5 kyr B.P., followed by a return to heavier values of ~ $-6.8‰$. A small $\delta^{13}CO_2$ peak also takes place at the start of SP-II, which coincides with a slightly smaller rate of CO_2 increase in the detailed *Monnin et al.* [2001] record. In a recent study, *Barker et al.* [2009] introduced the notion of "Heinrich Stadial 1" to characterize oceanic conditions during the first two SP; we will refer to this notion in the following.

[30] 1. SP-III (from 14.7 to 12.8 kyr B.P.), coincident with the Antarctic Cold Reversal (ACR) in the SH and the Bølling/Allerød (B/A) warm event in the NH, is marked by a progressive 3 ppmv decrease of CO_2, while a positive excursion culminating at $-6.5 \pm 0.1‰$ during the mid-SP-III (~14.1 kyr B.P.) is observed for $\delta^{13}CO_2$.

[31] 2. SP-IV (between 12.8 and 11.6 kyr B.P.), during which the Younger Dryas (YD) cold event in the NH and the post-ACR warming in the SH took place, reveals similar patterns for both CO_2 and $\delta^{13}CO_2$ as for SP-II. Thus, a progressive 13 ppmv CO_2 increase is observed until 12 kyr B.P., while a more abrupt rise of 10 ppmv is seen during the last 300 years. $\delta^{13}CO_2$ experiences a negative excursion of more than 0.2‰ amplitude, down to $-7.0 \pm 0.1‰$ (n = 6).

[32] 3. The EH (11.6 to 9 kyr B.P.) $\delta^{13}CO_2$ mean level is more ^{13}C-enriched than during SP-IV and amounts to $-6.8 \pm 0.1‰$ (n = 14). It also seems by $0.2 \pm 0.2‰$ more depleted in ^{13}C than at the end of LGM. In contrast, previous studies concluded to more enriched $\delta^{13}CO_2$ values during the Holocene (by 0.16‰ in SM1999 to $0.2 \pm 0.2‰$ [*Leuenberger et al.*, 1992]) than at the LGM. They were based on measurements performed on older LGM ice (Figure 1d), while Holocene data covered a different time window than considered here (from 9 to 7 kyr B.P., GICC05 age scale; see Figures 1d and 1e). In addition, the Holocene $\delta^{13}CO_2$ level may be subject to significant fluctuations, as pointed out by SM1999.

[33] Our measurements show that, although $\delta^{13}CO_2$ starts to decrease in parallel with the early CO_2 increase (a trend not captured in the less resolved SM1999 signal), its rapid drop takes place ~1 kyr later, when CO_2 has already increased by more than 10 ppmv. On the other hand, the EH $\delta^{13}CO_2$ rise appears more modest in our data set than in the TD record.

4. Discussion

[34] Despite the small size of the $\delta^{13}CO_2$ signal to be deciphered and the relatively small signal-to-noise ratio, some clear conclusions can now be drawn on its evolution during TI. Our more detailed EDC $\delta^{13}CO_2$ signal compared to the TD one supports some of the earlier conclusions drawn by SM1999. It also sheds some new light on the C cycle dynamics during the last deglaciation. The EDC

record highlights an overall W shape of atmospheric $\delta^{13}CO_2$ first broadly depicted by the SM1999 record throughout TI. It differs from SM1999 on the following patterns: (1) the two well-resolved minima taking place at times of steadily and important rises of CO_2 levels (late part of H1, and YD) reach comparable $\delta^{13}CO_2$ levels, around $-7.0‰$; (2) the CO_2 plateau accompanying the ACR goes together with a $\delta^{13}CO_2$ peak; (3) the average $\delta^{13}CO_2$ during the EH seems slightly more ^{13}C-depleted than at the end of LGM; and (4) SM1999 used a plot of $\delta^{13}CO_2$ as a function of the inverse of CO_2 (a so-called "Keeling plot," i.e., a mixing diagram where the y intercept should provide the isotopic composition of the added CO_2 in the atmosphere), taking all T-I data together to discuss the possible cause of the CO_2 increase. The improved time resolution of our data set permits us to subdivide T-I with distinct intercepts through time. A y intercept of $-6‰$ is obtained, similar to all deglacial data of SM1999, but only through SP-II and SP-III data (not shown). On the other hand, the two periods when CO_2 largely increases and $\delta^{13}CO_2$ simultaneously decreases in our record (SP-I and SP-IV) reveal another "Keeling plot" type of isotopic signature for the additional CO_2, similar for both subperiods: ~$-11‰$ (blue lines of Figure 2). The main conclusion of SM1999 that the C cycle behaved in a dual mode depending on the speed of climatic changes, i.e., a slow mode taking place during the EH and LGM, and a fast mode during TI, is thus not supported by the new Keeling plot (see Text S1).[1]

[35] The similar "Keeling plot" signature of SP-I and SP-IV suggests at first hand that the two main steps of atmospheric CO_2 increase during TI involved similar C cycle mechanisms. But their common y intercept cannot be directly interpreted as the isotopic signature of such mechanisms. Keeling plots work well only in an atmosphere-biosphere two-reservoir system experiencing fast exchanges [e.g., *Pataki et al.*, 2003]. On timescales of centuries to millennia such as during TI, the isotopic buffering effect of the ocean (air/sea exchanges, carbonate system) modifies the y intercept in a three-reservoir model, as shown for instance by [*Köhler et al.*, 2006a] using the preindustrial to industrial CO_2 increase and $\delta^{13}CO_2$ decrease as a case study. Therefore, other approaches are required to extract possible scenarios out of our new data set, relevant to carbon exchanges between the atmosphere, ocean and biosphere during TI. We use two of them here: a comparison with proxy records relevant to C cycle processes, and simulations of CO_2 and $\delta^{13}CO_2$ with two C cycle box models.

4.1. Comparison With Other C Cycle Proxy Records

[36] The good correlation between CO_2 and Antarctic deuterium throughout TI (Figures 1a and 1d), already noticed in numerous works [e.g., *Monnin et al.*, 2001; *Bianchi and Gersonde*, 2004], points toward a leading role of the Southern Ocean to drive the corresponding CO_2 evolution. As pointed out in the introduction, two types of Southern Ocean processes, a biological and a physical one, can be evoked.

---

[1]Auxiliary material is available with the HTML. doi:10.1029/2009GB003545.
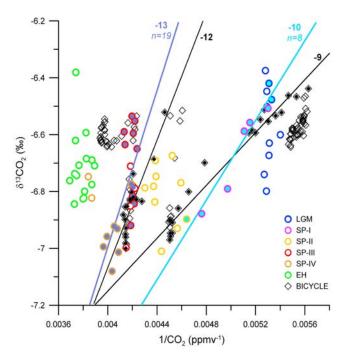
Figure 2. Mixing diagram depicting the relationship between atmospheric $\delta^{13}CO_2$ and the inverse of CO_2 (Keeling plot). The new data are shown as open circles with different colors, corresponding to the different subperiods defined in the main text. BICYCLE model output is represented by open black diamonds. Data points used for calculating the regression lines corresponding to the two periods of abrupt CO_2 rise and $\delta^{13}CO_2$ decline are filled with light blue (for the first ^{13}C dip) and dark blue (for the second ^{13}C dip). Filled black diamonds represent model results used for plotting the corresponding regression black lines. The y intercept values are shown next to the regression lines, together with the number data points. The y intercepts of the two rapid $\delta^{13}CO_2$ decreases give reasonably consistent values of $\sim -11‰$, comparable with the model results.

[37] According to the first one, the Southern Ocean during the LGM experienced a higher productivity due to higher atmospheric dust fluxes bringing more iron, a limiting micronutrient in high-nutrient low-chlorophyll (HNLC) regions [*Martin*, 1990]. As recorded in, e.g., EDC ice [*Lambert et al.*, 2008; *Gaspari et al.*, 2006] and shown in Figure 3a, the atmospheric dust (and iron) flux considerably decreases between ~18 and 14.6 kyr B.P., corresponding to the first half of the CO_2 deglacial increase. This would imply a decreasing biological pump in the Southern Ocean exporting less carbon to the ocean interior and thus increasing atmospheric CO_2. As phytoplankton preferentially assimilates the lighter carbon isotope (^{12}C), a decreasing productivity would be accompanied by a decreasing atmospheric $\delta^{13}CO_2$ [*Brovkin et al.*, 2002], in agreement with our record. During the second half of TI, the low dust values encountered in EDC ice suggest that the biologically mediated mechanism in the Southern Ocean did not influence the CO_2 and $\delta^{13}CO_2$ trends.

[38] The physical mechanism involves the rate of vertical mixing of the Southern Ocean: the cold LGM was associated with increased sea ice extent (mostly in winter) and with considerable stratification of the Southern Ocean water column [*Sigman and Boyle*, 2000; *Stephens and Keeling*, 2000; *Marchitto et al.*, 2007]. The deep Southern Ocean thus held a large amount of CO_2, due to organic matter remineralization, with a strongly ^{13}C-depleted signature originating from decomposed organic matter. *Duplessy et al.* [1988] showed that changes in Atlantic circulation at the end of LGM might have transferred low-$\delta^{13}C$ deep waters toward the ocean surface, a phenomenon validated subsequently by *Curry and Oppo* [2005]. Overall, the deglaciation, combining sea ice retreat, possible shifts of westerlies, and collapse of North Atlantic Deep Water (NADW) formation during its early phase, would have generated a Southern Ocean stratification breakdown and hence, the release of deep ocean ^{13}C-depleted CO_2 in the atmosphere, leading to an atmospheric CO_2 increase paralleled with a decrease of $\delta^{13}CO_2$ [e.g., *Toggweiler et al.*, 2006; *Menviel et al.*, 2008]. Such mechanism could have also acted during the YD, with a pause in between during the B/A, when the NADW was probably switched on again [*Knorr and Lohmann*, 2003]. As shown in Figure 3, several proxy records, matching the general shape of our $\delta^{13}CO_2$ record within their respective age model uncertainties, are in line with this physical scenario:

[39] 1. During the Heinrich Stadial 1 and YD, NADW formation got weakened [*Marchitto et al.*, 1998], as evidenced by an increased $^{231}Pa/^{230}Th$ ratio in North Atlantic sediments (Figure 3c) [*McManus et al.*, 2004]. This implies less NADW signal propagation toward the Southern Ocean waters.

[40] 2. NADW reduction is accompanied by a flushing of deep waters from the Southern Ocean into the Atlantic basin, thus equilibrating the water mass loss in the North Atlantic region. The nutrient-enriched and ^{13}C-depleted signal of old Antarctic-dwelled waters (e.g., Antarctic Intermediate Waters, AAIW) compared with deep waters from North Atlantic, is registered in North Atlantic marine sediments through two negative $\delta^{13}C$ excursions during the Heinrich Stadial 1 and YD [*Rickaby and Elderfield*, 2005] (Figure 3d).

[41] 3. A high-resolution $\Delta^{14}C$ record from the North Pacific [*Marchitto et al.*, 2007], shown in Figure 3e, reveals two negative excursions of more than 200‰ during the Heinrich Stadial 1 and the YD. They are interpreted as two episodes of transfer of old AAIW (including aged C of up to 4–5 kyr) into intermediate waters of the North Pacific, associated with the sea-ice retreat [*Stephens and Keeling*, 2000] and the Southern Ocean stratification breakdown [*Marchitto et al.*, 2007; *Schmittner et al.*, 2007]. This should be accompanied by the release of sequestered and ^{13}C-depleted deep oceanic carbon into the atmosphere. The scenario is corroborated at the start of TI by a low-resolution planktonic $\delta^{13}C$ record in subantarctic and equatorial Pacific [*Ninnemann and Charles*, 1997; *Spero and Lea*, 2002]. A recent high-resolution tropical Pacific planktic $\delta^{13}C$ record from *Stott et al.* [2009] also reveals a nice W trend throughout the deglaciation, reinforcing the scenario of
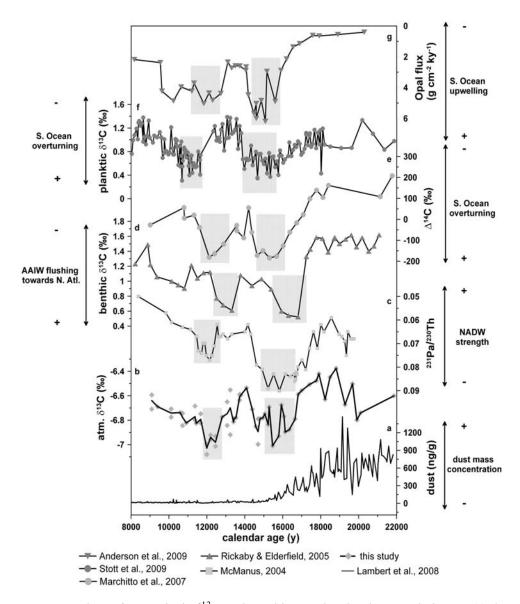
Figure 3. Comparison of atmospheric $\delta^{13}CO_2$ data with C cycle related tracers during TI: (a) dust concentration in the EDC core, taken as proxy of the biological pump G-IG patterns in the Southern Ocean [*Lambert et al.*, 2008]; (b) atmospheric $\delta^{13}CO_2$, from this study; (c) $^{231}Pa/^{230}Th$ in the subtropical North Atlantic, a tracer of North Atlantic Deep Waters formation strength [*McManus et al.*, 2004]; (d) benthic $\delta^{13}C$ in North Atlantic intermediate waters, reflecting the relative contribution between NADW and Antarctic intermediate waters throughout TI in the North Atlantic basin [*Rickaby and Elderfield*, 2005]; (e) $\Delta^{14}C$ data of intermediate waters in North Pacific, a proxy for Southern Ocean overturning strength [*Marchitto et al.*, 2007]; (f) planktonic $\delta^{13}C$ data from the western tropical Pacific [*Stott et al.*, 2009], also depicting changes in Southern Ocean G-IG overturning changes; (g) opal flux data from the Atlantic sector of the Southern Ocean, a proxy for Southern Ocean upwelling [*Anderson et al.*, 2009]. Atmospheric $\delta^{13}CO_2$ is plotted versus the Greenland GICC05 age scale, while the dust data are presented on the GICC05 ice scale. The oceanic proxies are on their original timescale. Shaded parts represent the cold periods of the Northern Hemisphere, as deduced from the individual timescales for each proxy.

G-IG Southern Ocean upwelling changes mentioned above (Figure 3f).

[42] 4. A high-resolution record of opal flux in the Southern Ocean [*Anderson et al.*, 2009], plotted in Figure 3g, shows an increase of upwelling strength in two steps, coincident with the Heinrich Stadial 1 and YD, thus also pointing toward increased ventilation of deep Southern Ocean waters as a main trigger of the two steps in the deglacial CO_2 increase.

[43] The physical mechanism involving Southern Ocean stratification breakdown in two episodes during TI thus qualitatively matches the CO_2 and $\delta^{13}CO_2$ trends, and could

also explain the common "Keeling plot" isotopic signature of the added carbon during the two episodes. Aside from the biological pump and ocean circulation hypotheses, a possibly straightforward explanation of the coevolution between CO_2 and $\delta^{13}CO_2$ concerns changes in Sea Surface Temperature (SST) during TI: due to isotopic fractionation during air/sea exchanges, a warmer ocean will leave a ^{13}C-enriched signal in the atmosphere. SM1999 assigned a large portion of their $\delta^{13}CO_2$ signal to this mechanism, by considering a globally averaged SST increase of 5°C between the LGM and EH. On the other hand, *Brovkin et al.* [2002], using the climate model CLIMBER-2, pointed out that the parallel changes of CO_2, alkalinity and bicarbonate ion concentration significantly affect the isotopic fractionation during air/sea exchanges, thus reducing the atmospheric $\delta^{13}CO_2$ imprint of SST changes. Moreover, the rapid $\delta^{13}CO_2$ changes observed in our record may be difficult to reconcile with the speed of SST changes in areas of deep water formation.

[44] SP-III encounters terrestrial carbon buildup in vegetation, soils and peat deposits [*MacDonald et al.*, 2006] which could have contributed to the small CO_2 decrease and to a positive $\delta^{13}CO_2$ anomaly in the atmosphere, as the biosphere preferentially assimilates ^{12}C. This is qualitatively corroborated by the CH_4 evolution (Figure 1c), pointing toward a switch-on of boreal wetland CH_4 emissions (requiring a concomitant intensification of the terrestrial C cycle) at that time [*Fischer et al.*, 2008]. Alternative scenarios attribute even more control of the $\delta^{13}CO_2$ variability by terrestrial biosphere carbon uptake and release as a consequence of abrupt temperature changes in the NH caused by the AMOC shutdown during H1 and YD [e.g., *Köhler et al.*, 2005b]. For the deglacial CO_2 rise, the contribution from progressively flooded continental shelves might also need some consideration [*Montenegro et al.*, 2006]; however, this scenario is challenged by the lag of the sea level increase with respect to CO_2 [*Pépin et al.*, 2001].

[45] In summary, the qualitative comparison of the EDC CO_2 and $\delta^{13}CO_2$ records with C cycle proxies suggest a dominant role of increased overturning in the Southern Ocean (as mainly evidenced by Δ^{14}C, opal flux and δ^{13}C records) during SP-I and SP-II to explain the two main steps of CO_2 increase, with an additional contribution of reduced biological pump during SP-I. The two mechanisms would have stalled during SP-III when NADW became stronger, and would also have been counterbalanced by terrestrial carbon buildup. To go further into a quantitative evaluation of mechanisms able to explain the CO_2 and $\delta^{13}CO_2$ signals, modeling is required. In the following, we explore the problem using two C cycle box models.

4.2. BICYCLE Model Runs

[46] We employed the BICYCLE model [*Köhler et al.*, 2005a], a coupled atmosphere/ocean/sediment/biosphere C cycle box model, run in a transient mode and forced with various time-dependent paleoclimatic data over TI. It consists of a single atmospheric box interacting with a 10 box ocean reservoir and the terrestrial biosphere, which is subdivided into seven compartments [*Köhler et al.*, 2005a]. The

ocean further communicates with a sediment reservoir. Mass balance equations are solved for the carbon stocks of the biospheric compartments, for DIC, TAlk, PO_4 and O_2 in the 10 oceanic reservoirs, for CO_2 in the atmosphere and for the carbon isotopes in all reservoirs.

[47] BICYCLE is the only C cycle model we are aware of which was run in transient mode over TI. It was also used for the interpretation of atmospheric carbon records and deep ocean δ^{13}C data over TI and much longer timescales of up to 2 Myr [*Köhler et al.*, 2005a, 2006a, 2006b; *Köhler and Fischer*, 2006; *Köhler and Bintanja*, 2008; *Köhler et al.*, 2010]. Since its application over TI [*Köhler et al.*, 2005a], improvements were performed in the parameterization of ocean circulation and sediment-ocean interaction, we thus use new simulation results, instead of the model output published by *Köhler et al.* [2005a].

4.2.1. Parameterizations

[48] The main model parameterizations, based on data obtained from ice core or marine cores (Figure 4) are the following:

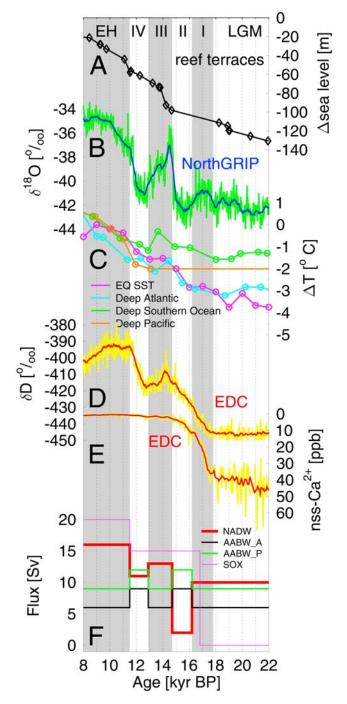[49] 1. Sea level rises by ~110m between 22 and 8 kyr B.P. based on reconstructions of coral reef terraces [*Fairbanks*, 1989] (Figure 4a). This leads to changes in the salinity, in the concentrations of all oceanic tracers and in the volumes of the oceanic boxes.

[50] 2. Temperature of all oceanic boxes is prescribed for present day from *Levitus and Boyer* [1994]. It changes over time according to oceanic proxy evidences for equatorial SST [*Visser et al.*, 2003] and deep ocean temperature [*Labeyrie et al.*, 1987] (Figure 4c). At high latitudes, it is represented by ice core isotopic profiles (North Atlantic and North Pacific: δ^{18}O on GICC05 age scale from North-GRIP [*North Greenland Ice Core Project Members*, 2004; *Andersen et al.*, 2007] (Figure 4b); Southern Ocean: δD (corrected for the effect of sea level rise) from EDC [*Parrenin et al.*, 2007; *Jouzel et al.*, 2001] synchronized to GICC05 [*EPICA Community Members et al.*, 2006; *Andersen et al.*, 2007], as shown in Figure 4d. Both ice core records are scaled to provide a SST ΔT of 4 K between the minimum glacial values and the present day.

[51] 3. Marine productivity in the Southern Ocean is scaled (if allowed by macronutrient availability) on dust input to the Southern Ocean as approximated by the non sea-salt-dust record measured in EDC [*Roethlisberger et al.*, 2002] (Figure 4e).

[52] 4. Ocean circulation between the 10 boxes for present conditions is parameterized with data from the World Ocean Circulation Experiment WOCE [*Ganachaud and Wunsch*, 2000] (Figure 4f). Compared to the initial BICYCLE runs over TI [*Köhler et al.*, 2005a], it was slightly modified to get a better agreement between simulated and reconstructed oceanic ^{13}C [*Köhler et al.*, 2010]. About 30% of the upwelled waters in the Southern Ocean are immediately redistributed to the intermediate equatorial Atlantic Ocean to account for the effect that, in the natural carbon cycle, upwelling waters in the Southern Ocean (which are then flowing as water masses of intermediate depth to the north) are still enriched in DIC [*Gruber et al.*, 2009]. Three major ocean currents are parameterized as follows (Figure 4f): (1) The strength of NADW (i.e., of its overturning [cf.

Köhler et al., 2005a]) is assumed to be about 40% weaker [*Meissner et al.*, 2003] during the LGM than at present day (10 versus 16 Sv), 2 Sv, 13 Sv and 11 Sv during the H1, B/A and YD, respectively [*McManus et al.*, 2004]. (2) Antarctic-dwelled waters (e.g., Antarctic Bottom Waters, AABW), penetrating both the deep Atlantic (AABW_A) and deep Pacific (AABW_P), is strengthened when NADW weakens (i.e., during H1 and YD) and vice versa (for B/A), considering the north-south opposite trend during these abrupt climatic changes [*Broecker*, 1998; *Rickaby and Elderfield*, 2005; *Kissel et al.*, 2008]: The EH and LGM AABW overall flux is set at of 15 Sv (6 SV for the Atlantic branch and 9 Sv for

the Pacific one); during H1 and YD (B/A), each section is strengthened (weakened) by 3 Sv. (3) Vertical mixing in the Southern Ocean (SOX) is set to 0 Sv during LGM in accordance with proxy evidence (e.g., $\delta^{13}C$ data from *Hodell et al.* [2003] and *Spero and Lea* [2002]); just after the dust proxy (non-sea-salt (nss)−Ca^{2+}) drop during SP-I, it is set to 15 Sv and maintained throughout B/A to be finally increased by another 5 Sv at the end of YD [*Köhler et al.*, 2005a].

[53]   5. Changes in the terrestrial biosphere carbon pool are assumed to be primarily temperature-dependent and made proportional to 3/4 of the NorthGRIP $\delta^{18}O$ and 1/4 of the EDC δD changes (taken as temperature proxies), reflecting the latitudinal distribution of vegetated land. The G-IG amplitude of land temperature change is considered as 8 K in the North and 5 K in the South. Net primary productivity is also parameterized on the modeled atmospheric CO_2 values to take into account CO_2 fertilization. More details on the terrestrial biosphere module can be found in the work of *Köhler and Fischer* [2004].

[54]   6. The additional effect of carbonate compensation [*Archer and Maier-Reimer*, 1994] to all temporal changing processes listed above is considered with a relaxation approach bringing the deep ocean carbonate ion concentration back to initial values.

[55]   All ice core records (isotopic temperature proxies and nss-dust) are implemented as 500 year running means in the different parameterizations.

4.2.2.   BICYCLE Model Output

[56]   Figure 5, left, illustrates the imprint Δ (with respect to the EH value) of major processes simulated with BICY-CLE, on atmospheric (Figure 5a) CO_2 and (Figure 5b) $\delta^{13}CO_2$. The reduction of Southern Ocean biological productivity (due to the onset of Fe limitation in HNLC [*Martin*, 1990]), as well as the Southern Ocean stratification breakdown [*Spero and Lea*, 2002] (associated with sea-ice retreat and decreasing salinity [*Watson and Naveira Garabato*, 2006; *Stephens and Keeling*, 2000]) are the main processes at work in the BICYCLE simulation at the TI inception, provoking a 15 and 22 ppmv CO_2 rise and a 0.20 and 0.32 ‰ $\delta^{13}CO_2$ decline, respectively.

Figure 4.   Proxy data sets used as BICYCLE input parameterizations. Shadings highlight the definition of subperiods given in the main text. (a) Coral reef terraces as indicator for sea level rise [*Fairbanks*, 1989]. (b) NorthGRIP $\delta^{18}O$ as northern high-latitude temperature proxy [*North Greenland Ice Core Project Members*, 2004]. (c) Changes in equatorial SST [*Visser et al.*, 2003] and deep ocean temperature in different oceanic compartments [*Labeyrie et al.*, 1987]. (d) EDC δD as southern high-latitude temperature proxy [*Jouzel et al.*, 2001]. (e) EDC non-sea-salt (nss) dust as proxy of aeolian iron input into the Southern Ocean [*Roethlisberger et al.*, 2002]. (f) Assumed changes in strengths of the main oceanic currents. For the cases shown in Figures 4b, 4d, and 4e, data show large short-term fluctuations; therefore a 500 year running mean is used in the simulations. All ice core records (Figures 4b, 4d, and 4e) are plotted versus the GICC05 age scale.
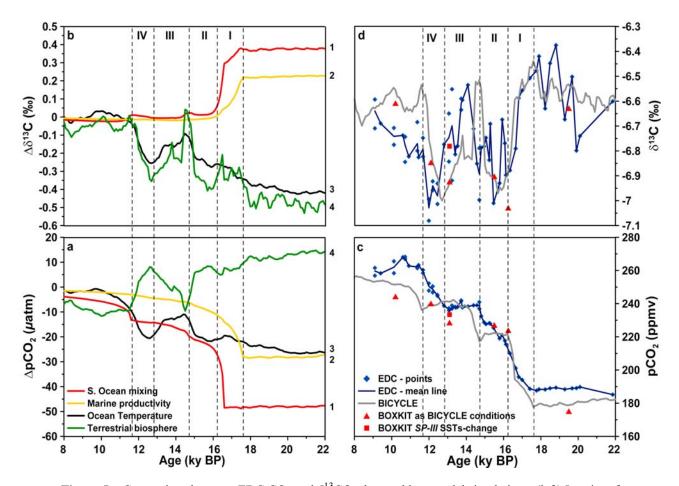
Figure 5. Comparison between EDC CO_2 and $\delta^{13}CO_2$ data and box model simulations. (left) Imprint of individual major C cycle processes on atmospheric (a) CO_2 and (b) $\delta^{13}CO_2$, simulated with the BICYCLE model. All curves express an anomaly ΔpCO_2 and $\Delta\delta^{13}C$ versus a reference corresponding to boundary EH conditions. The following processes are shown at this point: (1) Southern Ocean mixing; (2) marine productivity; (3) ocean temperature; and (4) terrestrial biosphere. (right) Superposition of the BICYCLE simulation integrating all individual processes of Figure 5 (left) (gray line) with our data (deep blue line and diamonds). The equilibrium-state BOXKIT model outputs, using similar boundary conditions as BICYCLE for each time period (red triangles) are also plotted for (c) CO_2 and (d) $\delta^{13}CO_2$. Red squares correspond to BOXKIT simulations using higher equatorial SST magnitudes. All series are plotted versus GICC05 age scale.

[57] During the NH cold events (H1 and YD), NADW weakens [*McManus et al.*, 2004], dampening the CO_2 increase and $\delta^{13}CO_2$ decrease related to AABW enhancement (+4.5 ppmv; −0.04‰) [*Rickaby and Elderfield*, 2005]; NADW (AABW) strengthening (weakening) at the end of SP-II and SP-IV, combined with stronger Southern Ocean water mixing at the end of YD, lead to a CO_2 outgassing of 10 and 7 ppmv, respectively (see Text S1).

[58] Sea level rise [*Fairbanks*, 1989] processes do not leave an important imprint on $\delta^{13}CO_2$ within the SPs, although they significantly affect CO_2 during the ACR, by provoking a 3 ppmv reduction (see Text S1). In contrast, vegetation growth, lagging Southern Ocean warming [*Hughen et al.*, 2004] and forced by CO_2 fertilization and NH warming, starts affecting $\delta^{13}CO_2$ during SP-II and becomes a major driver of this signal during SP-III and SP-IV (green

line of Figures 5a and 5b). The rise and fall of total biospheric carbon by 200PgC during SP-III and SP-IV, respectively [*Köhler and Fischer*, 2004; *Köhler et al.*, 2005a], lead to a 15 ppmv decrease and a 17 ppmv rise of CO_2, also causing a +0.35‰ and −0.40‰ $\delta^{13}CO_2$ anomaly. The response of atmospheric CO_2 to terrestrial C change is in corroboration with previous numerical studies: for example [*Scholze et al.*, 2003], assuming a total 180 PgC decline of terrestrial carbon pools during YD results in an atmospheric CO_2 rise of 30 ppmv due to land cooling and precipitation decline, both following the overturning circulation reduction. *Köhler et al.* [2005b] find, as a consequence of the AMOC shutdown and the accompanying Northern Hemispheric cooling, a total decline of terrestrial carbon pools of up to 140 PgC, resulting in peak-to-peak changes in atmospheric CO_2 and $\delta^{13}CO_2$ of 13 ppmv and 0.25‰, respectively. Recently, *Brovkin et al.* [2007] used a

model of intermediate complexity to evaluate the shared contributions of different C cycle mechanisms on CO_2 and $\delta^{13}CO_2$ G-IG changes. They conclude to relative imprints of ocean circulation, SST, land and marine productivity changes on $\delta^{13}CO_2$ very close to the BICYCLE results.

4.2.3. Data and Model Comparison

[59] The integrated signal from all the processes simulated with BICYCLE is compared with our data in Figure 5c for CO_2 and Figure 5d for $\delta^{13}CO_2$. Throughout TI, BICYCLE produces an increasing CO_2 trend, interrupted by phases of slower rate of increase or of stabilization, and accompanied by a marked $\delta^{13}CO_2$ W-shaped trend. The lowest $\delta^{13}CO_2$ is simulated during SP-II and SP-IV, with similar values around −7.0‰. A $\delta^{13}CO_2$ peak at the start of SP-III reaches ∼−6.5‰. BICYCLE thus captures the main features of the EDC records. A direct comparison of Keeling plots, obtained with the data and the simulations is provided in Figure 2. Similar y intercepts are obtained for the two main periods of abrupt CO_2 rise, suggesting that the sequence and amplitude of the involved processes are well captured by the model configuration. The Keeling plot comparison also highlights the limit of such plot, as the similar y intercepts generated by BICYCLE for the two periods come from a different combination of C cycle mechanisms at work.

[60] On the other hand, the timing of changes (for both CO_2 and $\delta^{13}CO_2$) can differ between observations and model outputs. The EDC $\delta^{13}CO_2$ peak of SP-III and the minimum of SP-IV appear earlier in the BICYCLE simulation. Both $\delta^{13}CO_2$ features mainly result from the terrestrial component in BICYCLE, itself mainly parameterized on NH temperature. As both EDC $\delta^{13}CO_2$ and the biosphere imprint in BICYCLE are on a common timescale (GICC05), the shift cannot be attributed to dating errors. One explanation lies in the time response of biospheric components to climate change being possibly underestimated in BICYCLE (a lag of ∼400 years, also found by *Scholze et al.* [2003]).

[61] Another data/model difference appears during SP-IV, when BICYCLE simulates a CO_2 plateau and a large $\delta^{13}CO_2$ increase whereas the EDC data reveal a steady increase and a minimum, respectively. Such BICYCLE output clearly depends on how well the timing and amplitude of SST and ocean circulation changes are parameterized during the YD and EH. As pointed out in section 4.1, C cycle proxy data suggest that the Southern Ocean mixing should have driven the YD CO_2 increase (it is parameterized as constant in the model), whereas the BICYCLE simulation gives more weight to terrestrial carbon release and SST increase.

[62] The box model bears other uncertainties and potential biases, such as (1) the relative dating of the various input signals and their synchronization with ice cores, (2) the pertinence of the proxies used for each process (e.g., the magnitude of oceanic fluxes throughout TI), and (3) the coarse spatial resolution of low latitudes. Still, it shows that the general shape of the EDC CO_2 and $\delta^{13}CO_2$ signals can be reproduced with a reasonable temporal sequence of C cycle mechanisms. It supports a scenario where Southern Ocean stratification breakdown and decrease of marine productivity jointly explain the early half of the CO_2 and $\delta^{13}CO_2$ signals, with the terrestrial biosphere intervening in the shape of both

signals during the B/A. The conclusion to be drawn for the YD episode is less clear, as the box model produces a $\delta^{13}CO_2$ minimum but fails to simulate the parallel CO_2 increase.

[63] A crucial point when comparing temporally highly resolved atmospheric records derived from ice cores with transient model simulations is that the gas records are smoothed by gas diffusion in the firn and by progressive bubble close-off. Therefore, they do not represent one single point in time, but are averaged over decades to centuries, mainly depending on accumulation rate and temperature. A gas diffusion and enclosure model [*Spahni et al.*, 2003] was used earlier to calculate the age distribution for CO_2 in EDC and the attenuation of atmospheric signals during the enclosure process. It has been calculated that the gas records represent averages between 213 (preindustrial) and 590 (LGM) years with a lognormal-shape-like age distribution [*Joos and Spahni*, 2008]. As a consequence, BICYCLE model simulations, which should represent atmospheric records before gas enclosure, might not be directly comparable with ice core records, especially for low accumulation sites and fast processes, because original atmospheric amplitudes are attenuated during the enclosure process [*Köhler et al.*, 2010]. A solution would be to proceed to similar measurements for the same time interval on a core with larger accumulation rate.

4.3. BOXKIT Model

[64] We also applied BOXKIT, a conceptual ocean/atmosphere model run under equilibrium states [*Paillard et al.*, 1993]. The ocean is split in 10 boxes: 5 for the surface, 2 for intermediate waters and 3 for the deep ocean. BOXKIT includes a single atmospheric box, but no terrestrial biosphere. The same forcings as BICYCLE are applied for six "snapshots" over TI.

[65] Similar overall trends as those of BICYCLE, both for CO_2 and $\delta^{13}CO_2$ are obtained (red squares in Figures 5c and 5d). As BOXKIT provides easier tuning than BICYCLE to carry on sensitivity tests, we used it to evaluate the output sensitivity to low latitude SST. Increasing tropical SSTs by 3°C (instead of 0.5°C as done for BICYCLE forcings) for the SP-III simulation, concomitantly with NH warming as is seen in North Atlantic sediment data from, e.g., *Lea et al.* [2003], leads to a $\delta^{13}CO_2$ increase by ∼0.2‰, more in line with the EDC data. This example shows the nonuniqueness of solutions when interpreting the C cycle data with box models.

5. Conclusions

[66] Our new record of $\delta^{13}CO_2$ from the EDC ice core over the last deglaciation reveals sharp fluctuations mostly associated with variations in the CO_2 rate of change. A comparison with other CO_2 and $\delta^{13}CO_2$ ice core data gives confidence in the validity of this new data set. In addition, consistent standard deviations are observed between different statistical approaches of the experimental system. The general shape of the deglacial $\delta^{13}CO_2$ signal can be summarized as a "W," with two minima accompanying the two major steps of CO_2 increase, and a peak when CO_2 gets stabilized or slightly decreasing.

[67] The comparison with C cycle related proxies highlights similarities with marine signals associated with the strength of Southern Ocean ventilation and upwelling, suggesting that this physical mechanism would be the main driver of the deglacial CO_2 increase.

[68] Two C cycle box models (BICYCLE and BOXKIT), run under the same input parameters support the dominant role of Southern Ocean physical processes and add the marine productivity decline during the early part of the deglaciation as another mechanism contributing to the $\delta^{13}CO_2$ decrease and CO_2 increase. The BICYCLE model supports an additional role of terrestrial carbon buildup to explain the CO_2 plateau and $\delta^{13}CO_2$ peak paralleling the ACR. It also simulates an early YD $\delta^{13}CO_2$ minimum followed by an increase to EH values, attributed to terrestrial carbon and SST decrease and subsequent increase, an explanation conflicting with C cycle proxy data which suggest a dominant role of strengthening Southern Ocean ventilation. The failure of BICYCLE to simulate a parallel CO_2 increase shows the limit of this modeling exercise, which crucially depends on assumptions regarding SO upwelling changes.

[69] More sophisticated approaches using coupled carbon-climate Earth system models will be needed in the future to better disentangle the contribution of each process, with their direct parameterizations in the models instead of the use of proxies. Our detailed EDC profile clearly highlights the need for fine time resolution in producing future $\delta^{13}CO_2$ records throughout major climatic events.

References

Ahn, J., M. Wahlen, B. L. Deck, E. J. Brook, P. A. Mayewski, K. C. Taylor, and J. W. C. White (2004), A record of atmospheric CO_2 during the last 40,000 years from the Siple Dome, Antarctica ice core, *J. Geophys. Res.*, *109*, D13305, doi:10.1029/2003JD004415.

Andersen, K. K., et al. (2007), The Greenland ice core chronology 2005, 15–42 ka. Part 1: Constructing the time scale, *Quat. Sci. Rev.*, *25*(23–24), 3246–3257.

Anderson, R. F., S. Ali, L. I. Bradtmiller, S. H. H. Nielsen, M. Q. Fleisher, B. E. Anderson, and L. H. Burckle (2009), Wind-driven upwelling in the Southern Ocean and the deglacial rise in atmospheric CO_2, *Science*, *323*(5920), 1443–1448, doi:10.1126/science.1167441.

Anklin, M., J.-M. Barnola, J. Schwander, B. Stauffer, and D. Raynaud (1995), Processes affecting the CO_2 concentrations measured in Greenland ice, *Tellus, Ser. B*, *47*, 461–470.

Archer, D., and E. Maier-Reimer (1994), Effect of deep-sea sedimentary calcite preservation on atmospheric CO_2 concentration, *Nature*, *367*(6460), 260–263, doi:10.1038/367260a0.

Archer, D., A. Winguth, D. Lea, and N. Mahowald (2000), What caused the glacial/interglacial atmospheric pCO_2 cycles? *Rev. Geophys.*, *38*(2), 159–189, doi:10.1029/1999RG000066.

Barker, S., P. Diz, M. J. Vautravers, J. Pike, G. Knorr, I. R. Hall, and W. S. Broecker (2009), Interhemispheric Atlantic seesaw response during the last deglaciation, *Nature*, *457*(7233), 1097–1102, doi:10.1038/nature07770.

Bereiter, B., J. Schwander, D. Lüthi, and T. F. Stocker (2009), Change in CO_2 concentration and O_2/N_2 ratio in ice cores due to molecular diffusion, *Geophys. Res. Lett.*, *36*, L05703, doi:10.1029/2008GL036737.

Bianchi, C., and R. Gersonde (2004), Climate evolution at the last deglaciation: The role of the Southern Ocean, *Earth Planet. Sci. Lett.*, *228*(3–4), 407–424, doi:10.1016/j.epsl.2004.10.003.

Broecker, W. S. (1998), Paleocean circulation during the last deglaciation: A bipolar seesaw?, *Paleoceanography*, *13*(2), 119–121, doi:10.1029/97PA03707.

Broecker, W. S., and T. H. Peng (1986), Carbon cycle: 1985 glacial to interglacial changes in the operation of the global carbon cycle, *Radiocarbon*, *28*(2A), 309–327.

Brook, E. J., S. Harder, J. Severinghaus, E. J. Steig, and C. M. Sucher (2000), On the origin and timing of rapid changes in atmospheric methane during the last glacial period, *Global Biogeochem. Cycles*, *14*(2), 559–572, doi:10.1029/1999GB001182.

Brovkin, V., M. Hofmann, J. Bendtsen, and A. Ganopolski (2002), Ocean biology could control atmospheric $\delta^{13}C$ during glacial-interglacial cycle, *Geochem. Geophys. Geosyst.*, *3*(5), 1027, doi:10.1029/2001GC000270.

Brovkin, V., A. Ganopolski, D. Archer, and S. Rahmstorf (2007), Lowering of glacial atmospheric CO_2 in response to changes in oceanic circulation and marine biogeochemistry, *Paleoceanography*, *22*, PA4202, doi:10.1029/2006PA001380.

Craig, H., Y. Horibe, and T. Sowers (1988), Gravitational separation of gases and isotopes in polar ice caps, *Science*, *242*(4886), 1675–1678, doi:10.1126/science.242.4886.1675.

Curry, W. B., and D. W. Oppo (2005), Glacial water mass geometry and the distribution of $\delta^{13}C$ of ΣCO_2 in the western Atlantic Ocean, *Paleoceanography*, *20*, PA1017, doi:10.1029/2004PA001021.

Dreyfus, G., J. Jouzel, M. L. Bender, A. Landais, V. Masson-Delmotte, and M. Leuenberger (2010), Firn processes and $\delta^{15}N$: Potential for a gas-phase climate proxy, *Quat. Sci. Rev.*, *29*, 28–42.

Duplessy, J. C., N. J. Shackleton, R. G. Fairbanks, L. Labeyrie, D. Oppo, and N. Kallel (1988), Deepwater source variations during the last climatic cycle and their impact on the global deepwater circulation, *Paleoceanography*, *3*(3), 343–360, doi:10.1029/PA003i003p00343.

EPICA Community Members, et al. (2006), One-to-one coupling of glacial climate variability in Greenland and Antarctica, *Nature*, *444*(7116), 195–198, doi:10.1038/nature05301.

Etheridge, D. M., L. P. Steele, R. L. Langenfelds, R. J. Francey, J.-M. Barnola, and V. I. Morgan (1996), Natural and anthropogenic changes in atmospheric CO_2 over the last 1000 years from air in Antarctic ice and firn, *J. Geophys. Res.*, *101*(D2), 4115–4128, doi:10.1029/95JD03410.

Fairbanks, R. G. (1989), A 17,000-year glacio-eustatic sea level record: Influence of glacial melting rates on the Younger Dryas event and deep-ocean circulation, *Nature*, *342*(6250), 637–642, doi:10.1038/342637a0.

Ferretti, D. F., D. C. Lowe, R. J. Martin, and G. W. Brailsford (2000), A new gas chromatograph-isotope ratio mass spectrometry technique for high-precision, N_2O-free analysis of $\delta^{13}C$ and $\delta^{18}O$ in atmospheric CO_2 from small air samples, *J. Geophys. Res.*, *105*(D5), 6709–6718, doi:10.1029/1999JD901051.

Fischer, H., et al. (2008), Changing boreal methane sources and constant biomass burning during the last termination, *Nature*, *452*(7189), 864–867, doi:10.1038/nature06825.

Flückiger, J., A. Dällenbach, T. Blunier, B. Stauffer, T. F. Stocker, D. Raynaud, and J.-M. Barnola (1999), Variations in atmospheric N_2O concentration during abrupt climatic changes, *Science*, *285*(5425), 227–230, doi:10.1126/science.285.5425.227.

Francey, R. J., C. E. Allison, D. M. Etheridge, C. M. Trudinger, I. G. Enting, M. Leuenberger, R. L. Langenfelds, E. Michel, and L. P. Steele (1999), A 1000-year high precision record of $\delta^{13}C$ in atmospheric CO_2, *Tellus, Ser. B*, *51*(2), 170–193, doi:10.1034/j.1600-0889.1999.t01-1-00005.x.

Friedli, H., H. Lötscher, H. Oeschger, U. Siegenthaler, and B. Stauffer (1986), Ice core record of the $^{13}C/^{12}C$ ratio of atmospheric CO_2 in the past two centuries, *Nature*, *324*(6094), 237–238, doi:10.1038/324237a0.

Ganachaud, A., and C. Wunsch (2000), Improved estimates of global ocean circulation, heat transport and mixing from hydrographic data, *Nature*, *408*(6811), 453–457, doi:10.1038/35044048.

Gaspari, V., C. Barbante, G. Cozzi, P. Cescon, C. F. Boutron, P. Gabrielli, G. Capodaglio, C. Ferrari, J. R. Petit, and B. Delmonte (2006), Atmospheric iron fluxes over the last deglaciation: Climatic implications, *Geophys. Res. Lett.*, *33*, L03704, doi:10.1029/2005GL024352.

Grachev, A. M., and J. P. Severinghaus (2003), Laboratory determination of thermal diffusion constants for $^{29}N_2/^{28}N_2$ in air at temperatures from −60 to 0 °C for reconstruction of magnitudes of abrupt climate changes using the ice core fossil-air paleothermometer, *Geochim. Cosmochim. Acta*, *67*(3), 345–360, doi:10.1016/S0016-7037(02)01115-8.

Gruber, N., et al. (2009), Oceanic sources, sinks and transport of atmospheric CO_2, *Global Biogeochem. Cycles*, *23*, GB1005, doi:10.1029/2008GB003349.

Hemming, S. R. (2004), Heinrich events: Massive late Pleistocene detritus layers of the North Atlantic and their global climate imprint, *Rev. Geophys.*, *42*, RG1005, doi:10.1029/2003RG000128.

Hodell, D. A., K. A. Venz, C. D. Charles, and U. S. Ninnemann (2003), Pleistocene vertical carbon isotope and carbonate gradients in the South Atlantic sector of the Southern Ocean. *Geochem. Geophys. Geosyst.*, *4*(1), 1004, doi:10.1029/2002GC000367.

Hughen, K. A., T. I. Eglinton, L. Xu, and M. Makou (2004), Abrupt tropical vegetation response to rapid climate changes, *Science*, *304*(5679), 1955–1959, doi:10.1126/science.1092995.

Intergovernmental Panel on Climate Change (2007), *Climate Change 2007: The Physical Science Basis. Contribution of Working Group 1 to the Fourth Assessment Report of the Intergovernmental Panel on Climate Change*, edited by S. Solomon et al., Cambridge Univ. Press, Cambridge, U. K.

Joos, F., and R. Spahni (2008), Rates of change in natural and anthropogenic radiative forcing over the past 20,000 years, *Proc. Natl. Acad. Sci. U. S. A.*, *105*(5), 1425–1430, doi:10.1073/pnas.0707386105.

Jouzel, J., et al. (2001), A new 27 ky high resolution east Antarctic climate record, *Geophys. Res. Lett.*, *28*(16), 3199–3202, doi:10.1029/2000GL012243.

Jouzel, J., et al. (2007), Orbital and millennial Antarctic climate variability over the past 800,000 years, *Science*, *317*(5839), 793–796, doi:10.1126/science.1141038.

Kissel, C., C. Laj, A. M. Piotrowski, S. L. Goldstein, and S. R. Hemming (2008), Millennial-scale propagation of Atlantic deep waters to the glacial Southern Ocean, *Paleoceanography*, *23*, PA2102, doi:10.1029/2008PA001624.

Knorr, G., and G. Lohmann (2003), Southern Ocean origin for resumption of Atlantic thermohaline circulation during deglaciation, *Nature*, *424*, 532–536, doi:10.1038/nature01855.

Köhler, P., and R. Bintanja (2008), The carbon cycle during the mid Pleistocene transition: The Southern Ocean decoupling hypothesis, *Clim. Past*, *4*, 311–332.

Köhler, P., and H. Fischer (2004), Simulating changes in the terrestrial biosphere during the last glacial/interglacial transition, Global Planet. Change, *43*(1–2), 33–55, doi:10.1016/j.gloplacha.2004.02.005.

Köhler, P., and H. Fischer (2006), Simulating low frequency changes in atmospheric CO_2 during the last 740,000 years, *Clim. Past*, *2*(2), 57–78.

Köhler, P., H. Fischer, G. Munhoven, and R. E. Zeebe (2005a), Quantitative interpretation of atmospheric carbon records over the last glacial termination, *Global Biogeochem. Cycles*, *19*, GB4020, doi:10.1029/2004GB002345.

Köhler, P., F. Joos, S. Gerber, and R. Knutti (2005b), Simulated changes in vegetation distribution, land carbon storage, and atmospheric CO_2 in response to a collapse of the North Atlantic thermohaline circulation, *Clim. Dyn.*, *25*, 689–708, doi:10.1007/s00382-005-0058-8.

Köhler, P., H. Fischer, J. Schmitt, and G. Munhoven (2006a), On the application and interpretation of Keeling plots in paleo climate research-deciphering $\delta^{13}C$ of atmospheric CO_2 measured in ice cores, *Biogeosciences*, *3*, 539–556.

Köhler, P., R. Muscheler, and H. Fischer (2006b), A model-based interpretation of low-frequency changes in the carbon cycle during the last 120,000 years and its implications for the reconstruction of atmospheric $\Delta^{14}C$, *Geochem. Geophys. Geosyst.*, *7*, Q11N06, doi:10.1029/2005GC001228.

Köhler, P., H. Fischer, and J. Schmitt (2010), Atmospheric $\delta^{13}CO_2$ and its relation to pCO_2 and deep ocean $\delta^{13}C$ during the last Pleistocene, *Paleoceanography*, *25*, PA1213, doi:10.1029/2008PA001703.

Labeyrie, L. D., J. C. Duplessy, and P. L. Blanc (1987), Variations in mode of formation and temperature of oceanic deep waters over the past 125,000 years, *Nature*, *327*(6122), 477–482, doi:10.1038/327477a0.

Lambert, F., B. Delmonte, J. R. Petit, M. Bigler, P. R. Kaufmann, M. A. Hutterli, T. F. Stocker, U. Ruth, J. P. Steffensen, and V. Maggi (2008), Dust-climate couplings over the past 800,000 years from the EPICA Dome C ice core, *Nature*, *452*(7187), 616–619, doi:10.1038/nature06763.

Lea, D. W., D. K. Pak, L. C. Peterson, and K. A. Hughen (2003), Synchroneity of tropical and high-latitude Atlantic temperatures over the last glacial termination, *Science*, *301*(5638), 1361–1364, doi:10.1126/science.1088470.

Leuenberger, M., U. Siegenthaler, and C. C. Langway (1992), Carbon isotope composition of atmospheric CO_2 during the last ice age from an Antarctic ice core, *Nature*, *357*(6378), 488–490, doi:10.1038/357488a0.

Levitus, S., and T. P. Boyer (1994), *World Ocean Atlas*, vol. 4, *Temperature, NOAA Atlas NESDIS 4*, 117 pp., U.S. Dept. of Comm., Washington, D. C.

Loulergue, L., F. Parrenin, T. Blunier, J.-M. Barnola, R. Spahni, A. Schilt, G. Raisbeck, and J. Chappellaz (2007), New constraints on the gas age-ice age difference along the EPICA ice cores, 0–50 kyr, *Clim. Past*, *3*(3), 527–540.

Loulergue, L., A. Schilt, R. Spahni, V. Masson-Delmotte, T. Blunier, B. Lemieux, J.-M. Barnola, D. Raynaud, T. F. Stocker, and J. Chappellaz (2008), Orbital and millennial-scale features of atmospheric CH_4 over the past 800,000 years, *Nature*, *453*(7193), 383–386, doi:10.1038/nature06950.

Lourantou, A. (2009), Constraints on the carbon dioxide deglacial rise based on its stable carbon isotopic ratio, Ph.D. thesis, 194 pp., Univ. Joseph Fourier, Grenoble, France.

MacDonald, G. M., D. W. Beilman, K. V. Kremenetski, Y. Sheng, L. C. Smith, and A. A. Velichko (2006), Rapid early development of circumarctic peatlands and atmospheric CH_4 and CO_2 variations, *Science*, *314*(5797), 285–288, doi:10.1126/science.1131722.

Marchitto, J. T. M., W. B. Curry, and D. W. Oppo (1998), Millennial-scale changes in North Atlantic circulation since the last glaciation, *Nature*, *393*(6685), 557–561, doi:10.1038/31197.

Marchitto, T. M., S. J. Lehman, J. D. Ortiz, J. Flückiger, and A. van Geen (2007), Marine radiocarbon evidence for the mechanism of deglacial atmospheric CO_2 rise, *Science*, *316*(5830), 1456–1459, doi:10.1126/science.1138679.

Martin, J. H. (1990), Glacial-interglacial CO_2 change: The iron hypothesis, *Paleoceanography*, *5*(1), 1–13, doi:10.1029/PA005i001p00001.

McManus, J. F., R. Francois, J.-M. Gherardi, L. D. Keigwin, and S. Brown-Leger (2004), Collapse and rapid resumption of Atlantic meridional circulation linked to deglacial climate changes, *Nature*, *428*(6985), 834–837, doi:10.1038/nature02494.

Meissner, K. J., A. Schmittner, A. J. Weaver, and J. F. Adkins (2003), Ventilation of the North Atlantic Ocean during the Last Glacial Maximum: A comparison between simulated and observed radiocarbon ages, *Paleoceanography*, *18*(2), 1023, doi:10.1029/2002PA000762.

Menviel, L., A. Timmermann, A. Mouchet, and O. Timm (2008), Climate and marine carbon cycle response to changes in the strength of the Southern Hemispheric westerlies, *Paleoceanography*, *23*, PA4201, doi:10.1029/2008PA001604.

Monnin, E., A. Indermühle, A. Dällenbach, J. Flückiger, B. Stauffer, T. F. Stocker, D. Raynaud, and J.-M. Barnola (2001), Atmospheric CO_2 concentrations over the last glacial Termination, *Science*, *291*(5501), 112–114, doi:10.1126/science.291.5501.112.

Montenegro, A., M. Eby, J. O. Kaplan, K. J. Meissner, and A. J. Weaver (2006), Carbon storage on exposed continental shelves during the glacial-interglacial transition, *Geophys. Res. Lett.*, *33*, L08703, doi:10.1029/2005GL025480.

North Greenland Ice Core Project Members (2004), High-resolution record of Northern Hemisphere climate extending into the last interglacial period, *Nature*, *431*(7005), 147–151, doi:10.1038/nature02805.

Ninnemann, U. S., and C. D. Charles (1997), Regional differences in Quaternary subantarctic nutrient cycling: Link to intermediate and deep water ventilation, *Paleoceanography*, *12*(4), 560–567, doi:10.1029/97PA01032.

Obata, A. (2007), Climate carbon cycle model response to freshwater discharge into the North Atlantic, *J. Clim.*, *20*(24), 5962–5976, doi:10.1175/2007JCLI1808.1.

Paillard, D., M. Ghil, and H. L. Treut (1993), Dissolved organic mater and the glacial-interglacial pCO_2 problem, *Global Biogeochem. Cycles*, *7*(4), 901–914, doi:10.1029/93GB02013.

Paillard, D., L. Labeyrie, and P. Yiou (1996), Macintosh program performs time-series analysis, *Eos Trans. AGU*, *77*(39), 379, doi:10.1029/96EO00259.

Parrenin, F., et al. (2007), The EDC3 chronology for the EPICA Dome C ice core, *Clim. Past*, *3*(3), 485–497.

Pataki, D. E., J. R. Ehleringer, L. B. Flanagan, D. Yakir, D. R. Bowling, C. J. Still, N. Buchmann, J. O. Kaplan, and J. A. Berry (2003), The

application and interpretation of Keeling plots in terrestrial carbon cycle research, *Global Biogeochem. Cycles*, *17*(1), 1022, doi:10.1029/2001GB001850.

Pépin, L., D. Raynaud, J.-M. Barnola, and M. F. Loutre (2001), Hemispheric roles of climate forcings during glacial-interglacial transitions as deduced from the Vostok record and LLN-2D model experiments, *J. Geophys. Res.*, *106*(D23), 31,885–31,892, doi:10.1029/2001JD900117.

Rasmussen, S. O., et al. (2006), A new Greenland ice core chronology for the last glacial termination, *J. Geophys. Res.*, *111*, D06102, doi:10.1029/2005JD006079.

Rickaby, R. E. M., and H. Elderfield (2005), Evidence from the high-latitude North Atlantic for variations in Antarctic Intermediate water flow during the last deglaciation, *Geochem. Geophys. Geosyst.*, *6*, Q05001, doi:10.1029/2004GC000858.

Roethlisberger, R., R. Mulvaney, E. W. Wolff, M. A. Hutterli, M. Bigler, S. Sommer, and J. Jouzel (2002), Dust and sea salt variability in central East Antarctica (Dome C) over the last 45 kyrs and its implications for southern high-latitude climate, *Geophys. Res. Lett.*, *29*(20), 1963, doi:10.1029/2002GL015186.

Schmittner, A., E. Brook, and J. Ahn (2007), Impact of the ocean's overturning circulation on atmospheric CO_2, in *Ocean Circulation: Mechanisms and Impacts*, *Geophys. Monogr. Ser.*, vol. 173, edited by A. Schmittner, J. Chiang, and S. Hemmings, 209–246, AGU, Washington, D. C.

Scholze, M., W. Knorr, and M. Heimann (2003), Modelling terrestrial vegetation dynamics and carbon cycling for an abrupt climatic change event, *Holocene*, *13*(3), 327–333, doi:10.1191/0959683603hl625rp.

Schulz, M., D. Seidov, M. Sarnthein, and K. Stattegger (2001), Modeling ocean-atmosphere carbon budgets during the Last Glacial Maximum: Heinrich 1 meltwater event-Bølling transition, *Int. J. Earth Sci.*, *90*, 412–425, doi:10.1007/s005310000136.

Schwander, J., J.-M. Barnola, C. Andrié, M. Leuenberger, A. Ludin, D. Raynaud, and B. Stauffer (1993), The age of the air in the firn and the ice at Summit, Greenland, *J. Geophys. Res.*, *98*(D2), 2831–2838, doi:10.1029/92JD02383.

Severinghaus, J. P., A. Grachev, and M. Battle (2001), Thermal fractionation of air in polar firn by seasonal temperature gradients, *Geochem. Geophys. Geosyst.*, *2*(7), 1048, doi:10.1029/2000GC000146.

Sigman, D., and E. Boyle (2000), Glacial/interglacial variations in atmospheric carbon dioxide, *Nature*, *407*(6806), 859–869, doi:10.1038/35038000.

Smith, H. J., H. Fischer, M. Wahlen, D. Mastroianni, and B. Deck (1999), Dual modes of the carbon cycle since the Last Glacial Maximum, *Nature*, *400*(6741), 248–250, doi:10.1038/22291.

Spahni, R., J. Schwander, J. Flückiger, B. Stauffer, J. Chappellaz, and D. Raynaud (2003), The attenuation of fast atmospheric CH_4 variations recorded in polar ice cores, *Geophys. Res. Lett.*, *30*(11), 1571, doi:10.1029/2003GL017093.

Spero, H. J., and D. W. Lea (2002), The cause of carbon isotope minimum events on glacial terminations, *Science*, *296*(5567), 522–525, doi:10.1126/science.1069401.

Stephens, B. B., and R. F. Keeling (2000), The influence of Antarctic sea ice on glacial-interglacial CO_2 variations, *Nature*, *404*(6774), 171–174, doi:10.1038/35004556.

Stott, L., J. Southon, A. Timmermann, and A. Koutavas (2009), Radiocarbon age anomaly at intermediate water depth in the Pacific Ocean during the last deglaciation, *Paleoceanography*, *24*, PA2223, doi:10.1029/2008PA001690.

Toggweiler, J. R. (1999), Variation of atmospheric CO_2 by ventilation of the ocean's deepest water, *Paleoceanography*, *14*(5), 571–588, doi:10.1029/1999PA900033.

Toggweiler, J. R., J. L. Russell, and S. R. Carson (2006), Midlatitude westerlies, atmospheric CO_2, and climate change during the ice ages, *Paleoceanography*, *21*, PA2005, doi:10.1029/2005PA001154.

Trudinger, C. M., L. G. Enting, D. M. Etheridge, R. J. Francey, V. A. Levchenko, L. P. Steele, D. Raynaud, and L. Arnaud (1997), Modeling air movement and bubble trapping in firn, *J. Geophys. Res.*, *102*(D6), 6747–6763, doi:10.1029/96JD03382.

Tschumi, J., and B. Stauffer (2000), Reconstructing past atmospheric CO_2 concentration based on ice-core analyses: Open questions due to in situ production of CO_2 in the ice, *J. Glaciol.*, *46*(152), 45–53, doi:10.3189/172756500781833359.

Visser, K., R. Thunell, and L. Stott (2003), Magnitude and timing of temperature change in the Indo-Pacific warm pool during deglaciation, *Nature*, *421*(6919), 152–155, doi:10.1038/nature01297.

Watson, A. J., and A. C. Naveira Garabato (2006), The role of Southern Ocean mixing and upwelling in glacial-interglacial atmospheric CO_2 change, *Tellus, Ser. B*, *58*(1), 73–87, doi:10.1111/j.1600-0889.2005.00167.x.

J. Chappellaz, J. V. Lavrič, A. Lourantou, and D. Raynaud, Laboratoire de Glaciologie et Géophysique de l'Environnement, Université Joseph Fourier–Grenoble, CNRS, 54 rue Molière, F-38402 St Martin d'Hères, France. (chappellaz@lgge.obs.ujf-grenoble.fr)

P. Köhler, Alfred Wegener Institute for Polar and Marine Research, Am Handelshafen 12, D-27570 Bremerhaven, Germany.

E. Michel and D. Paillard, Laboratoire des Sciences du Climat et de l'Environnement, IPSL, Université Versailles-St Quentin, CNRS, Orme des Merisiers, Bat. 701, F-91191 Gif-sur-Yvette, France.